Quantitative seismic analysis of a thin layer of CO_2 in the Sleipner injection plume

G. A. Williams[1]* & R. A. Chadwick[1]

[1]British Geological Survey, Keyworth, Nottingham, NG12 5GG

*Corresponding author. Tel: +44-115-9363130; fax: +44-115-9363437

ABSTRACT

Time-lapse seismic reflection data have proved to be the key monitoring tool at the Sleipner CO_2 injection project. Thin layers of CO_2 in the Sleipner injection plume, show striking reflectivity on the time-lapse data, but the derivation of accurate layer properties, such as thickness and velocity remains very challenging. This is because the rock physics properties are not well-constrained nor are CO_2 distributions on a small scale. However, because the reflectivity is dominantly composed of interference wavelets, from thin layer tuning, the amplitude and frequency content of the wavelets can be diagnostic of their temporal thickness. A spectral decomposition algorithm based on the Smoothed Pseudo Wigner-Ville Distribution has been developed. This enables single frequency slices to be extracted with sufficient frequency and temporal resolution to provide diagnostic spectral information on individual CO_2 layers. The topmost layer of CO_2 in the plume is particularly suitable for this type of analysis because it is not affected by attenuation from overlying CO_2 layers and because there are areas where it is temporally isolated from deeper layers. Initial application of the algorithm to the topmost layer shows strong evidence of thin layer tuning effects. Analysis of tuning frequencies on high resolution 2D data suggests that layer two-way

temporal thicknesses in the range 6 to 11 milliseconds (ms) can be derived with an accuracy of 1 to 2 ms. Direct measurements of reflectivity from the top and the base of the layer permit calculation of layer velocity, with values of around 1470 ms^{-1}, in reasonable agreement with existing rock physics estimates. The frequency analysis can, therefore, provide diagnostic information on layer thicknesses in the range 4 to 8 metres. The method is currently being extended to the full 3D time-lapse datasets at Sleipner.

BACKGROUND

Thin layers of CO_2 in the Sleipner injection plume show striking reflectivity on the time-lapse data, but the derivation of accurate layer properties, such as thickness and velocity remains very challenging.

It is well known that geological strata produce characteristic frequency tuning of propagating seismic waves, such that thin beds cause enhancement or suppression of preferred frequencies within the seismic spectrum depending on their temporal (travel-time) thickness. Spectral decomposition is a signal processing technique that allows the seismic signal to be decomposed into discrete frequency components, allowing spectral tuning effects to be evaluated (Partyka et al. 1999). A number of authors have used spectral decomposition both qualitatively and quantitatively to characterize stratigraphical sequences on the basis of their frequency content (e.g. Chakraborty & Okaya 1995; Partyka et al. 1999; Sinha et al. 2005; Wang 2007; Chen et al. 2008). In many cases, certain of the decomposed frequency components allow enhanced imaging of fine-scale stratigraphical and depositional features (e.g Partyka et al. 1999; Laughlin et al. 2003).

In this paper we examine the possibility of using spectral decomposition in a quantitative manner to assess the thickness and velocities of thin layers of dense-phase carbon dioxide in the injected CO_2 plume at Sleipner in the Norwegian North Sea. Early work on the Sleipner time-lapse 3D seismic data used seismic amplitudes and time-shift analysis to estimate layer thicknesses (e.g. Arts et al 2004; Chadwick et al 2004, 2005; Ghaderi & Landrø, 2009), but this depended on deriving velocities from rock physics, with significant uncertainty. An alternative approach used structural analysis of the reservoir topseal topography to determine the thickness of the topmost CO_2 layer (Chadwick et al 2009; Chadwick & Noy 2010), but this gave no information on layer velocities. Pre and post-stack inversions have been used to derive layer properties (e.g. Delépine et al. 2009), but these are not highly-constrained and cannot properly account for the strong modulation of reflection amplitudes by the thin layers. More recently a constrained AVO technique has been tested where forward modeling was used to extract layer thicknesses from offset raypaths, again with inconclusive results (Sturton et al. 2010).

This paper describes some initial findings from detailed analysis of the seismic waveforms associated with the thin layers, in particular by analyzing their spectral content. We look at the 3D time-lapse data and also some of the high resolution 2D data acquired over the Sleipner CO_2 plume.

TIME-LAPSE SEISMIC IMAGING OF THE SLEIPNER CO_2 PLUME

CO_2 separated from natural gas produced at the Sleipner field (Norwegian block 15/9) is being injected into the Utsira Sand, a regional saline aquifer of late Cenozoic age, in excess of 200 m thick in the Sleipner area (Figure 1a). The aquifer comprises mostly clean

unconsolidated sand of high porosity (> 0.3) and permeability (> 1 Darcy). A number of thin intra-reservoir mudstones, typically 1 – 2 m thick, are evident from geophysical logs acquired in wells around Sleipner (Figure 1b).

The CO_2 is injected in a dense phase via a deviated well at a depth of 1012 m below sea level, approximately 200 m beneath the top of the reservoir. Injection commenced in 1996 at a roughly constant rate, with around 13 million tons of CO_2 stored by 2011. A comprehensive deep-focused monitoring program has been deployed, utilizing a number of geophysical methods (Arts et al 2008). Of these, time-lapse seismic has proven to be the key monitoring tool. A baseline 3D survey was acquired in 1994, with repeat surveys in 1999, 2001, 2004, 2006, 2008 and 2010. In addition, a 2D high resolution survey was acquired over the plume in 2006.

The plume is imaged on the seismic data as a number of high amplitude sub-horizontal reflections within the aquifer (Figure 2). Most of this reflectivity is thought to represent tuned responses from thin layers of CO_2 trapped beneath the intra-reservoir mudstones which are partially but not wholly sealing. The reflective layering had formed by 1999 with each individual reflection traceable on all of the subsequent surveys. As a general rule the middle and upper reflections in the plume have increased in amplitude and lateral extent on successive time-lapse surveys, whereas the lower layers have ceased growing and in some cases have shrunk and dimmed. The plume is around 200 m in height and markedly elliptical in plan view (Figure 2).

A key objective of the Sleipner monitoring project is to demonstrate that geological storage of CO_2 is a safe and verifiable technology. This requires that quantitative constraints can be

placed on dynamic flow simulations of the injection process. The injection well is near-horizontal at the injection point, so no wellbore penetrates either the CO_2 plume or the stratigraphy that the plume now occupies. Quantitative analysis is therefore challenging. Early work based on detailed interpretation and mapping, established amplitude-thickness tuning relationships for the reflective layers (e.g. Arts et al 2004; Chadwick et al. 2004, 2005). This was a reasonable approach for the early surveys when layers were thin, but localized decreases in layer reflectivity on more recent vintages suggest that in places the tuning thickness is now being exceeded. In addition, reflections from the lower layers have become strongly attenuated. This is thought, at least in part, to reflect more fundamental seismic imaging problems in the deeper plume. A further limitation of simple amplitude – thickness modeling is that it requires reasonably accurate knowledge of layer velocities. This is not readily available. Velocities can be obtained from rock physics, but in the absence of any independent constraints (no wellbore penetrates any of the CO_2 layers), the rock physics is uncertain. The properties of CO_2 in the Utsira reservoir (where conditions are close to the critical point for CO_2) are very sensitive to temperature and pressure, and the former in particular is somewhat uncertain (Alnes et al. 2010).

The topmost CO_2 layer

Much of the recent quantitative analyses have focused on the topmost CO_2 layer in the plume (Figure 3). There are two main reasons for this. Firstly the layer lies directly beneath the reservoir topseal, and due to the lack of overlying CO_2, it is clearly and stably imaged with no progressive signal attenuation through time. Secondly, the layer spreads by buoyancy-driven lateral CO_2 migration and ponding beneath the topseal topography. The latter can be mapped with reasonable accuracy, as uncertainties largely reside with overburden velocities which are

constrained by nearby wells.

By 2006 the topmost layer was well-developed, forming an irregular shaped accumulation some 3 km from south to north and about 0.8 km from east to west (Figure 3). Layer thicknesses can be estimated directly on a trace-by-trace basis by taking the difference in elevation between the topseal relief, and the spatially interpolated CO_2 – water contact on the same trace, with no requirement to know the velocity of the CO_2 layer itself (Chadwick et al. 2009; Chadwick & Noy 2010). In this study topseal relief was calculated using a constant overburden velocity of 1857 ms^{-1} (as found in the nearby well 15/9-13). Computed values are quite 'jittery' due to small, noise-related travel-time offsets, so a 50 x 50 m spatial smoothing filter was applied (Figure 4a). Reflection amplitudes correspond broadly but not exactly to the calculated thicknesses (Figure 4b). A prominent north-trending prolongation corresponds to northward migration of the CO_2 beneath and along a linear ridge in the topseal surface (Figures 3 and 4).

This paper investigates the potential application of time-frequency analysis to further improve understanding of layer thicknesses and velocities in the Sleipner plume, with particular reference to the topmost CO_2 layer. We focus on the 2006 time-lapse seismic data because a high resolution 2D dataset is also available.

ESTIMATING THE THICKNESS OF THIN LAYERS USING TIME-FREQUENCY ANALYSIS

For a thin layer sitting in a homogeneous background medium, peak seismic amplitude of the tuned reflection wavelet occurs when the reflection from the layer top exhibits maximum constructive interference with the (reverse polarity) reflection from the layer base. This occurs

when the layer two-way thickness corresponds to half of the dominant seismic wavelength. The two way temporal tuning thickness (T) corresponds to half of the dominant seismic period. If the velocity (V) of the layer is known, the tuning thickness can also be expressed as a true (one-way) depth thickness (t). Tuning also occurs when the layer thickness is 3/2, 5/2, 7/2 etc times the seismic wavelength (corresponding to the 2nd, 3rd, 4th etc tuning peaks).

Thus for a wavelet of dominant frequency (F_{DOM}) and a layer velocity (V):

$$T = \frac{1}{2*F_{DOM}} \quad \text{Equation 1a}$$

$$t = \frac{V}{4*F_{DOM}} \quad \text{Equation 1b}$$

Tuning thickness is therefore a function of the dominant frequency in the seismic wavelet. Of more specific interest here is the fact that discrete frequencies within the wavelet frequency spectrum will be preferentially enhanced by thin layer tuning. This provides us with a potential diagnostic tool.

This is illustrated by synthetic seismic modeling of a simple wedge model of varying temporal thickness (Figure 5). The seismic wavelet is extracted from the Sleipner 3D data, with a frequency range roughly between 15 and 55 Hz, centered on 35 Hz. At layer temporal thickness greater than the tuning thickness (~14ms) the layer is resolved as two separate reflections from the top and bottom interfaces. Beneath the tuning thickness the wavelet sidelobes from the top and base interfaces interfere and the wedge is imaged as an interference wavelet whose amplitude and frequency content vary with layer thickness (Figure 5a). The frequency response of the synthetic seismogram (Figure 5b) shows the seismic

response at discrete frequencies. For example, on the first tuning peak, temporal thicknesses of 10 ms and 25 ms produce tuning at frequencies of 50 Hz and 20 Hz respectively. For this particular wavelet f_{dom} = 35 hz (see later) the second tuning peak ($T = 3/2f_{dom}$) only starts to influence the signal at wedge thicknesses above about 24 ms, with the third tuning peak only significant at even greater thicknesses.

It has been shown that the amplitude spectrum of the layer reflection computed over a short time window is a composite of the wavelet spectrum and the tuning effect of the layer (Partyka et al. 1999). The temporal thickness of a layer can therefore be estimated by identifying the tuning frequency from the discrete frequency components extracted from the time-windowed seismic trace, given appropriate spectral balancing to remove wavelet overprint (Partyka et al. 1999; Mahendra et al. 2006). With accurate layer velocity information the true (depth) thickness of the layer can also be established.

The Wigner-Ville Distribution

In order to extract spectral information from single reflections from individual layers in the Sleipner plume it is necessary to analyze very narrow travel-time windows (25 ms or less). Conventional linear time-frequency analysis techniques such as the Windowed Fourier Transform and Continuous Wavelet Transform suffer from resolution problems. A narrow analysis window localizes the spectrum in time but provides poor frequency resolution, whereas a broader window loses temporal accuracy. The Wigner-Ville Distribution (a member of the quadratic Cohen Class of time-frequency transforms) can potentially overcome some of the limitations inherent in these techniques (Li & Zheng 2008). The improved resolution offered by quadratic transforms (Figure 6) make them particularly suitable for calculating the

thickness of individual CO_2 layers in the Sleipner plume, which can only be satisfactorily isolated using a short time window.

Although less popular than the various linear transforms, the Wigner-Ville Distribution (WVD) has been applied to the spectral decomposition of both active and passive seismic signals (Li & Zheng 2008; Wu & Liu 2006; Prieto et al. 2005). The WVD function (see Wigner (1932), and Ville (1948) for a complete formulation) is calculated by computing the power spectrum of a signal (the Fourier transform of the wavelet auto-correlation function) and removing the integration over time (Equation 2). In effect the WVD is constructed by computing the auto-correlation over all possible lags at each time sample (the local auto-correlation function) and transforming into Fourier space.

$$W_{x(t,v)} = \int_{-\infty}^{+\infty} x\left(t+\frac{\tau}{2}\right) x^*(t-\frac{\tau}{2}) e^{-i2\pi v\tau} d\tau \qquad \text{Equation 2}$$

Where W_x is the Wigner distribution of a function x, t is time, τ the lag, v the frequency and * represents complex conjugation.

The result is a quadratic function. As a consequence of this, discrete events in a time series will produce cross-terms in the time-frequency distribution (Figure 6d). The cross-terms can be reduced by smoothing with an appropriate filter kernel along the time g(x-t) and frequency h(τ) axes (Equation 3) to give the Smoothed Pseudo Wigner-Ville Distribution (SPWVD).

$$SPWVD_{x(t,v)} = \int_{-\infty}^{+\infty} h(\tau) \int_{-\infty}^{+\infty} g(x-t) x\left(t+\frac{\tau}{2}\right) x^*\left(t-\frac{\tau}{2}\right) dt\, e^{-i2\pi v\tau} d\tau \qquad \text{Equation 3}$$

Smoothing leads to reduced resolution in both the time and frequency planes forcing a trade-off between resolution and interference effects (Figure 7).

Synthetic data example

In order to investigate the potential of the SPWVD to map thin layer tuning effects comparable to those observed on the Sleipner seismic data, a 2D synthetic seismic model was created. Rock physics data based on core measurements and geophysical well logs from the Utsira Sand were used to calculate the key seismic properties (Table 1). Velocities for the sand – water – CO_2 system were calculated for both uniform and patchy fluid mixing, using, respectively, the Reuss and Hill averages (Figure 8).

The model comprised a thin sand layer saturated with CO_2 trapped beneath mudstone caprock in a simple 2D domal closure (Figure 9), and assuming uniform fluid mixing. The geometry of the CO_2 layer is modeled as a 2D dome (or ridge) increasing in thickness from zero at the edges to 12 m at the apex (the latter corresponding to a two-way temporal thickness of about 17 ms for high CO_2 saturations).

The seismic section was generated by 1D convolution with a Ricker wavelet of dominant frequency 50 Hz, similar to the high resolution 2D data from Sleipner (see below). Strong tuning is evident on the flanks of the structure with maximum tuning of the full wavelet at a layer thickness of 6 m (corresponding to a temporal thickness of 8.4 ms) which is consistent with the 60 Hz dominant frequency (Equation 1a). In the central part of the model the tuning thickness is exceeded and the CO_2 layer is explicitly imaged as separate negative and positive reflections from the top and base of the layer respectively.

A set of iso-frequency sections through the model were computed using the SPWVD to demonstrate thin-bed effects on the time-frequency spectrum (Figure 10). The tuning thickness, corresponding to the peak amplitude of the power spectrum and highlighted with a black arrow, clearly decreases with increased frequency. Thus at a discrete frequency of 30 Hz, tuning occurs at the layer crest (t = 12 m), whereas at progressively higher frequencies the tuning peak migrates down the flanks of the dome as the layer progressively thins, with the 70Hz section showing tuning at about 5 m layer thickness. It is clear therefore, that given sufficient bandwidth in the input data, the SPWVD is capable of quantifying bed thickness within the expected range for the CO_2 layers at Sleipner (<10 m).

APPLICATION TO SLEIPNER SEISMIC DATA

In the following section we present preliminary observations from the spectral decomposition applied to the Sleipner 3D and 2D high resolution seismic datasets from 2006. This is not a systematic or exhaustive analysis of the results but rather an insight into some of the preliminary findings.

The 3D data occupy a rectangular area some 6 km x 3 km, covering the current footprint of the CO_2 plume (Figure 11a). The 2D lines are arranged in a radial configuration centered on the plume, plus a number of parallel lines NNE-SSW and one E-W. Comparison of the 3D and 2D data (Fig. 11b & c) show the higher resolution of the latter, but at the expense of rather higher noise levels. These differences are confirmed by the frequency spectra (Fig. 12a). The 3D data have a dominant frequency of around 35 Hz with useful frequencies up to around 75 Hz or so, whereas the 2D data peak around 50 Hz, but with useful energy above 100 Hz. It is

notable that the low noise levels of the 3D data allow even its upper frequency limits to be usefully exploited (see below).

Evidence of frequency tuning on the 3D data

Full spectral analysis of the 3D datasets is ongoing and beyond the scope of this initial paper. Here we restrict discussion to preliminary analysis which does show clear evidence of frequency tuning associated with changes in CO_2 layer thickness.

Discrete frequency cubes were generated from the 3D data from 30 to 80 Hz at 5 Hz intervals. To correct for the fact that the frequency spectrum of the seismic wavelet is not flat, spectral balancing was required. For the purposes of this preliminary analysis a simple normalization scheme was adopted – for each frequency slice the maximum amplitude seen across all of the seismic traces was scaled to a common value.

Particularly distinctive tuning effects on the topmost layer are evident at the southern end of the prominent north-trending ridge of CO_2 (Figure 13a). Discrete frequency slices (computed using the SPWVD with a 24 point Hanning window) along a west-east section (Figure 13b) show low frequency tuning (~40-50 Hz) at the ridge crest, with higher frequency tuning peaks progressively migrating down the ridge flanks. This tuning behavior is strikingly similar to that of the synthetic 2D domal model shown in Figures 9 and 10. Reference to the tuning curves (Figure 13c) suggests therefore that the CO_2 layer has a temporal thickness of around 12 ms at the ridge crest, thinning to around 6 ms at the 80 Hz tuning peak. Characterization of the even thinner outermost flanks of the ridge would require frequencies above 80 Hz, which are beneath the noise floor of the dataset.

Estimating CO_2 layer temporal thickness through spectral analysis

The 2D data is significantly higher frequency than the 3D data with a relatively flat spectrum in the 10 -75 Hz range and useful frequencies beyond 100 Hz (Figure 12a). As a consequence, it is reasonable to use a simple amplitude normalization procedure to balance each spectral slice. Two intersecting seismic sections (STO698-07001 & STO698-06006) traversing the topmost CO_2 layer from north to south and northeast to southwest, were chosen for spectral analysis (for location see Figure 11a). Coincident sections were extracted from the 3D data for comparison. The 3D sections were balanced using wavelet spectra extracted over a large time window through the 3D volume (Figure 12a).

2D seismic line STO698-07001 and co-incident 3D data

The wavelet trough (blue on Figure 14a) marking the negative impedance contrast at the top of the topmost CO_2 layer was picked and also the corresponding peak (red on Figure 14a) marking the base of the layer. It is clear that the layer has a somewhat variable temporal thickness. In the north and the south, where the layer thickens progressively from zero at its edges, the measured trough-to-peak temporal separation is notably consistent at ~7 to 8 ms (Figure 14b), indicative of a tuning wavelet closely matching the trough-to- peak separation of the seismic wavelet (Figure 12b). Here, in the tuning region, changes in layer thickness are manifest principally as changes in reflection amplitude. Where the CO_2 is thickest however (at 250-600 m distance in Figure 14), the tuning thickness is exceeded and the high frequency content of the data has allowed the top and base of the CO_2 layer to be imaged explicitly. In these regions we can measure the true peak-to-trough time separation which ranges up to

10.5 ms; the systematic nature of these changes in temporal thickness can be clearly seen when plotted (Figure 14b).

The SPWVD was used to compute a time-frequency volume in a 24 sample Hanning window about the topmost CO_2 reflector and a sequence of iso-frequency sections were extracted from the time-frequency distribution (Figure 15). Tuning frequencies increase from the centre of the section where layer thickness is greatest, out to the northern and southern ends of the section where layer thicknesses decrease. Thus tuning frequencies around 40-50 Hz dominate in the central parts, around 65 – 70 Hz on the mid flanks and around 75Hz towards the ends of the section. This situation is directly comparable with the synthetic 2D dome model (Figures 9 and 10) in which CO_2 has accumulated in a topographic culmination, with a roughly flat CO_2 - water contact.

The tuning frequencies (the frequency with the highest amplitude at each trace) extracted from the SPWVD can be converted into layer temporal thicknesses via Equation 1a. There is a good correlation between the calculated and measured temporal thicknesses (Figure 14b) although the former are some 1 - 2 ms larger than the measured values between 300 and 500 m distance. This discrepancy probably reflects frequency smoothing inherent in the SPWVD, although inaccuracies in time picking could also contribute to the mismatch.

2D seismic line STO698-06006 and co-incident 3D data

Spectral decomposition (using the SPWVD with a 24 sample Hanning window) was also applied to 2D line STO698-06006, which images a culmination of the top reservoir surface (Figure 16). For passive infill of caprock topography, the CO_2 layer will be thickest at this

point, at a distance of about 500 m (Figure 16b). The measured trough-to-peak temporal separation (filled black circles on Figure 16b) increases from the tuning value of about ~ 7 ms at the southwestern end of the profile to ~10 ms at 500 m. Again, there is a good correlation between the measured temporal thicknesses and temporal thickness estimates based on the spectral analysis from the 2D data (solid black line in Figure 16b). Thickness estimates derived from the spectrally balanced coincident 3D section also show a reasonable match with the observed temporal separations.

The sequence of iso-frequency sections along the 2D line (Figure 17) again show that the tuning frequency increases from the centre of the topographic high (at ~500 m distance) to its flanks.

Both of the examples indicate that tuning frequencies extracted from the SPWVD can provide a direct measure of the temporal thickness of the CO_2. Where the CO_2 layer is thickest, the 2D high resolution data allow the frequency-derived values to be compared with direct trough-to-peak measurements. It is clear that the lower frequency 3D data can also provide useful information with this technique, provided an appropriate spectral balancing procedure is adopted.

CO_2 LAYER VELOCITY

Temporal thickness estimates can be converted to layer thickness provided the velocity of the CO_2 saturated layer is known. Velocity can be estimated from rock physics (Figure 8), but seismic parameters can be subject to significant uncertainty. For the high resolution 2D seismic data, velocity can be derived directly from the reflectivity of the topmost CO_2 layer where the top and base reflections show temporal separation. This exploits the fact that the

CO_2 layer is overlain by caprock (water-saturated mudstone) with different acoustic properties to those of the underlying rock (water-filled sand) (Figure 18).

For reflection at the top of the layer:

$$R_{TOP} = \frac{A_1 - A_2}{A_1 + A_2} \qquad \text{Equation 4}$$

and for reflection at the base of the layer:

$$R_{BASE} = \frac{A_2 - A_3}{A_2 + A_3} \qquad \text{Equation 5}$$

Where:

R_{TOP} = reflection co-efficient at the layer top

R_{BASE} = reflection co-efficient at the layer base

A_1 = acoustic impedance of the caprock

A_2 = acoustic impedance of the CO_2 saturated sand in the layer

A_3 = acoustic impedance of water – saturated sand beneath the layer

Equations 4 and 5 rearrange into a quadratic equation solving for A_2 in terms of A_1, A_3 and the ratio R_{TOP}/R_{BASE}. The latter is approximately equal to the ratio of the reflection amplitudes from the top and base of the reflector and so can be measured directly from the seismic data. The acoustic impedances of the caprock and virgin aquifer are also available from well-logs and so A_2 can be calculated. The coefficients (A, B, C) in the quadratic are given by:

$$A = 1 - \frac{R_{TOP}}{R_{BASE}} \qquad \text{Equation 6}$$

$$B = (A_3 - A_1) * \left(1 + \frac{R_{TOP}}{R_{BASE}}\right) \qquad \text{Equation 7}$$

$$C = A_1 * A_3 * \left(\frac{R_{TOP}}{R_{BASE}} - 1\right) \qquad \text{Equation 8}$$

The ratio of the amplitudes of the reflections from the top and base of the layer was measured for the central part of STO698-07001 where the tuning thickness is exceeded. It varies between approximately 1.05 and 1.8 but with a well-defined mode of ~1.35 and a mean of 1.37 (Figure 18b). The variation will likely reflect minor lateral changes in acoustic properties but is principally due to noise. Taking this ratio as approximating to R_{TOP} / R_{BASE} we can say:

$R_{TOP} / R_{BASE} = 1.37$

Measured values of V_P and density (Table 1) give acoustic impedances for the caprock and water-saturated Utsira Sand as follows:

$A_1 = 4.88 \times 10^6$ ms^{-1}.kgm^{-3}

$A_3 = 4.20 \times 10^6$ ms^{-1}.kgm^{-3}

From these the acoustic impedance of the CO_2 -saturated sand is given by the positive solution of the quadratic:

$A_2 = 2.85 \times 10^6$ ms^{-1}.kgm^{-3}

In order to derive V_P for the CO_2 – saturated sand it is necessary to know its density which

depends on the CO_2 saturation. Core experiments on the Utsira Sand (Erik Lindeberg personal communication 2003) indicate very low residual water saturations under drainage conditions, with layers greater than 2 m thick having average CO_2 saturations in the range 0.8 to 0.9 (Chadwick et al. 2005). Again using the parameters from Table 1, CO_2 saturations of 0.9 and 0.8 give whole-rock densities of 1934 and 1947 kgm^{-3} respectively. These translate into V_P values for the CO_2 – saturated sand of 1474 and 1464 ms^{-1} respectively. This is in good agreement with the values determined from the rock physics (Figure 8) and provides an independent calibration of the rock physics velocity calculation. It is the case however that derived velocities are very sensitive to the input properties of the overlying and underlying strata and we consider that uncertainties are currently too high for firm conclusions to be drawn regarding fluid mixing scales. More robust assessments of the key velocity and density parameters of the virgin sand and the immediately overlying caprock are required and this is planned for the next phase of work.

CO_2 LAYER THICKNESSES

The CO_2 saturated layer velocity values derived above can be combined with the results of the spectral analysis to estimate true thicknesses in the topmost CO_2 layer. Along the 2D seismic lines temporal layer thicknesses approach 10 ms around the structural culmination of the layer. This converts to a layer true thickness of ~7 to 7.5 m. This is in good agreement with the 7 to 8 m range derived from structural analysis of the topseal (Figure 4a). It is important to stress that the latter does not utilize the CO_2 layer velocity and so is a wholly independent estimate. Away from the structural culmination a reasonable match is maintained down to thicknesses of 4 to 5m, with temporal thicknesses of about 6 ms. The latter corresponds to a frequency of 80 Hz (Figure 13c) which roughly marks the maximum usable

frequency in the data. Thicknesses less than about 4 or 5 m cannot be characterized by the peak tuning / frequency content.

CONCLUSION

Thin layers of CO_2 in the Sleipner injection plume are dominantly imaged as tuned wavelets and are potentially suitable for the use of spectral analysis in assessing their temporal thickness. A spectral decomposition algorithm based on the Smoothed Pseudo Wigner-Ville Distribution enables single frequency slices to be extracted with sufficient frequency and temporal resolution to provide diagnostic spectral information on an individual CO_2 layer. The algorithm has been tested on 2D data but is equally applicable to 3D data. Initial investigations suggest that for the topmost layer in the plume temporal thicknesses can be derived with an accuracy of 1 – 2 ms. On high resolution 2D data the layer is locally above the tuning thickness and measurement of top and base layer reflectivity permits direct calculation of layer velocity. These values are in close agreement with the rock physics.

The work illustrates the potential, but also the significant challenges of deriving reliable properties for these thin layers. The topmost layer of the plume is rather suitable for this type of analysis because, as it spreads beneath the topseal there are large areas on several of the time-lapse datasets where it is not closely underlain by a deeper reflective layer. This enables the pure wavelet to be isolated for frequency analysis. Deeper in the plume the layers are very closely spaced. Their wavelets doubtless interfere, both above and below, significantly affecting the accuracy of the method. Ongoing work is concentrating more on quantitative analysis of the 3D datasets, looking at time-lapse changes in frequency signature and how these can be related to changing layer thicknesses. This is potentially a powerful approach

because the independent information on topmost layer thicknesses based on structural analysis of the topseal topography (Chadwick & Noy 2010) gives the possibility of deriving true layer velocities within the tuning domain.

ACKNOWLEDGMENTS

This publication has been produced with support from the CO2ReMoVe Project and the BIGCCS Centre, whom thank for permission to publish. CO2ReMoVe is funded by the EU 6th Framework Programme and by industry partners BP, ConocoPhillips, ExxonMobil, Statoil, Schlumberger, Total, Vattenfall and Wintershall. BIGCCS is part of the Norwegian research program Centres for Environment-friendly Energy Research (FME) and is funded by the Research Council of Norway and an industrial consortium: Aker Solutions, ConocoPhilips, Det Norske Veritas AS, Gassco AS, Hydro Aluminium AS, Shell Technology AS, Statkraft Development AS, Statoil Petroleum AS and TOTAL E&P Norge AS. The authors publish with the permission of the Executive Director, British Geological Survey (NERC).

References

Alnes H, Eiken O, Nooner S, Sasagawa G, Stenvold T and Zumberge M, 2011, Results from Sleipner gravity monitoring: updated density and temperature distribution of the CO_2 plume. Energy Procedia, 4 (2011), 5504-5511.

Arts, R.J., Chadwick, R.A., Eiken, O., Thibeau, S. and S Nooner, 2008, Ten years' experience of monitoring CO_2 injection in the Utsira Sand at Sleipner, offshore Norway: First Break, 26, 65 – 72.

Arts, R., Eiken, O., Chadwick, R.A., Zweigel, P., Van Der Meer, L. and B. Zinszner, 2004, Monitoring of CO_2 injected at Sleipner using time-lapse seismic data: Energy, 29, 1383-1393.

Chadwick, R.A., Arts, R. Eiken, O. Kirby, G.A., Lindeberg, E. and P. Zweigel, 2004, 4D seismic imaging of a CO_2 bubble at the Sleipner Field, central North Sea, *in* R.J. Davies, J.A. Cartwright, S.A. Stewart, M. Lappin M and J.R. Underhill , eds., 3-D Seismic Technology: Application to the Exploration of Sedimentary Basins, Geological Society, London (2004), 311-320.

Chadwick, R.A., Arts, R. and O. Eiken, 2005, 4D seismic quantification of a CO_2 plume at Sleipner, North Sea, *in* A.G. Dore and B. Vining, eds., Petroleum Geology: North West Europe and Global Perspectives : Proceedings of the 7th Petroleum Geology Conference, Published by the Geological Society, London, 1385 – 1399.

Chadwick, R.A., D. Noy, R. Arts, and O. Eiken, 2009, Latest time-lapse seismic data from

Sleipner yield new insights into CO_2 plume development, *in* Energy Procedia, Volume 1, Issue 1: Greenhouse Gas Control Technologies 9, Proceedings of the 9th International Conference on Greenhouse Gas Control Technologies, Washington DC (2009), 2103-2110.

Chadwick, R.A. and D.J. Noy, 2010, History – matching flow simulations and time-lapse seismic data from the Sleipner CO_2 plume, *in* A.G. Dore and B. Vining, eds., Petroleum Geology: North West Europe and Global Perspectives: Proceedings of the 7th Petroleum Geology Conference, Published by the Geological Society, London.

Chakraborty, A. and David Okaya, 1995, Frequency-time decomposition of seismic data using wavelet-based methods, Geophysics, 60, 1906-1916.

Chen, G., Matteucci, G., Fahmy, B. and Chris Finn, 2008, Spectral-decomposition response to reservoir fluids from a deepwater West Africa reservoir, Geophysics 73(6), 23-30.

Delépine, N., Clochard, V., Labat, K., Ricarte, P., and C. Le Bras, 2009, Stratigraphic inversion for CO_2 monitoring purposes - A case study for the saline aquifer of Sleipner Field: 71st EAGE Conference & Exhibition, Amsterdam, The Netherlands

Ghaderi, A. and Martin Landrø, 2009, Estimation of thickness and velocity changes of injected carbon dioxide layers from prestack time-lapse seismic data, Geophysics 74(2), 17-28.

Laughlin, K., Garossino, P. and G. Partyka, 2003, Spectral decomposition for seismic stratigraphic patterns: Search and Discovery, article 40096,4 pp, http://www.searchanddiscovery.net/documents/geophysical/2003/laughlin/index.htm

Li., Y, and X. Zheng, 2008, Spectral decomposition using Wigner-Ville distribution with applications to carbonate reservoir characterization: The Leading Edge, 27(8), 1050-1057.

Mahendra, K., Sharma, S., Kumar, B., and A. Srivastava, 2006, An Approach to Net Thickness Estimation Using Spectral Decomposition: Geohorizons, 11(1), 58-62.

Partyka, G., Gridley, J. And J. Lopez, 1999, Interpretational applications of spectral decomposition in reservoir characterization: The Leading Edge, 18(3), 353-360.

Prieto, G. A., Vernon, F.L., Masters, G. and D. J. Thomson, 2005, Multitaper Wigner-Ville Spectrum for Detecting Dispersive Signals from Earthquake Records: Proceedings of the Thirty-Ninth Asilomar Conference on Signals, Systems, and Computers, Pacific Grove, CA., 938-941.

Sinha, S., Routh, P. S., Anno, P. D. and John P. Castagna, 2005, Spectral Decomposition of Seismic Data with Continuous-Wavelet Transform, Geophysics, 70(6), 19-25.

Sturton, S., Buddensiek, M. L. and M. Dillen, 2010, AVO Analysis of Thin Layers – Application to CO_2 Storage at Sleipner: 72nd EAGE Conference & Exhibition incorporating SPE EUROPEC 2010, Barcelona, Spain, 14 - 17 June 2010.

Ville, J., 1948, Théorie et applications de la notion de signal analytique. Cable Transmission 2A, 61–74.

Wang, Y., 2007, Seismic time frequency spectral decomposition by matching pursuit, Geophysics, 72(1), 13-20.

Wigner, E.P. 1932, On the quantum correction for thermodynamic equilibrium, Physical Review, 40, 749–759.

Wu, X. and T. Liu, 2006, Spectral decomposition of seismic data with reassigned smoothed pseudo Wigner-Ville distribution: Journal of Applied Geophysics, 68, 386-393.

Figure Captions

Figure 1 a) Isopach map of the Utsira Sand b) geophysical well log from the vicinity of Sleipner. The reservoir sand has characteristically low γ-ray (GR) readings and higher neutron porosity (NPHI). The γ-ray peaks (neutron porosity troughs) within the sand denote thin mudstones.

Figure 2 Top panels show a cross-section from the time-lapse 3D seismic data at Sleipner showing the baseline (1994) dataset and a selection of the repeat surveys. Note strong reflections corresponding to the CO_2 plume with the topmost layer arrowed. Bottom panels show map views of the plume expressed as total reflection amplitude. Black polygons mark the extent of the topmost CO_2 layer within the overall plume footprint.

Figure 3 3D views of the top of the Utsira reservoir looking northwest. a) Shaded relief display of the reservoir top. b) Reservoir top with superimposed reflection amplitude of topmost layer of CO_2 in 2001. (c) Reservoir top with superimposed reflection amplitude of topmost layer of CO_2 in 2006. Note the prominent north-trending tongue of CO_2 which migrates beneath a linear ridge in the basal topseal surface.

Figure 4 Map views of the topmost layer of CO_2 in 2006. a) Layer thickness calculated trace-by-trace from difference in elevation of the CO_2 - water contact and the overlying base topseal (smoothed on 50 x 50 m spatial filter). b) Reflection amplitudes.

Figure 5 Seismic response of a simple low velocity wedge. a) 2D seismic section showing reflectivity tuning where wedge temporal thickness is less than 14 ms. b) 2D seismic section

as in (a) but showing reflectivity as a function of frequency. Lines show the 1st, 2nd and 3rd tuning peaks computed from Equation 1a.

Figure 6 a) Synthetic trace comprising four Ricker wavelets with peak frequencies of 80, 60, 40 and 20 Hz. Frequency decomposition using b) the windowed Fourier Transform (computed in a 128 point Hanning window), (c) the Continuous Wavelet Transform and (d) the Wigner-Ville distribution.

Figure 7 a) Synthetic trace comprising four Ricker wavelets with peak frequencies of 80, 60, 40 and 20 Hz. Frequency decomposition using (b) the Wigner-Ville Distribution and (c) the Smoothed Pseudo Wigner-Ville Distribution (smoothed using a 24 point Hanning window). Note that the obvious interference cross-terms present in (b) have been smoothed out at the expense of time-frequency resolution in (c).

Figure 8 Calculated rock physics parameters (V_P and density) for the rock-water-CO_2 system for the Utsira Sand using the Reuss and Hill averages for the uniform and patchy mixing bounds respectively. Values of VP derived from layer reflection ratios (see below) are shown as a black line.

Figure 9 Synthetic model of a thin layer with 100% CO_2-saturated sand trapped beneath a 2D domal closure, and enclosed by water-saturated strata. Model assumes a Ricker wavelet of dominant frequency 60 Hz. a) Velocity/density model. (b) Synthetic seismic section from 1D convolution. The thick black traces on both flanks show the tuning thickness for the seismic wavelet used in the convolution. The zone between 0.4 and 0.5 s has been decomposed into a sequence of time-frequency slices shown in Figure 10.

Figure 10 Iso-frequency sections at 30, 40, 50, 60, and 70 Hz computed using the SPWVD with a 24 point Hanning window for the 2D domal model shown in Figure 9. Individual seismic traces are superimposed on the time-frequency plot. Arrows indicate the tuning thickness (for a layer velocity of 1428 m/s) at the extracted frequency.

Figure 11 a) Map showing coverage of the 2006 3D survey (rectangle) and the 2006 2D high resolution lines (black lines), with the reflection footprint of the 2006 plume shown for reference. The areal extent of the top layer of CO_2 is shown by a black line. The locations of the seismic profiles in Figures 14 and 16 are shown as thick white lines. b) 3D seismic section through the upper plume. c) 2D high resolution data along the same line of section as (b).

Figure 12 Plot of the smoothed power spectrum (a) and truncated autocorrelation (b) for the 3D (dashed line) and 2D (solid line) seismic datasets. The truncated autocorrelation of a trace provides the amplitude characteristics of the wavelet's Fourier transform. Power spectra were extracted over a large time window (800-1500 ms) for traces outside the plume and averaged to produce an estimate of the wavelet spectrum. Note that the peak-to-trough separations of the 3D and 2D wavelets are ~13 ms and ~7 ms respectively.

Figure 13 Tuning at the southern end of the CO_2-filled ridge. a) Map view (looking north) of the top of the Utsira reservoir, showing the outer extents of the topmost CO_2 layer in 2006 (black line) and the line of cross-section. b) Discrete frequency slices from the 3D data on a west–east cross-section through the north-trending ridge of CO_2 (computed using the SPWVD with a sliding 24 point Hanning window). c) Tuning curves showing the relationship between frequency and two-way temporal thickness.

Figure 14 Part of 2D line STO698-07001. a) Seismic section showing picks on the top and base of the top CO_2 layer (for location see Figure 11a). b) Plots of temporal thickness and reflection amplitudes for the seismic section. The blue and red lines show RMS amplitudes extracted from a 4 ms window about the top and base reflector respectively. The filled black circles show the measured peak-trough time separation, while the solid black line and broken black line show temporal thickness estimates derived from spectral decomposition of the 2D and a coincident (spectrally balanced) 3D seismic profile. Spectral decomposition employed the SPWVD with a sliding 24 point Hanning window.

Figure 15 Normalized iso-frequency sections extracted from the time-frequency distribution computed in a 24 point Hanning window about the topmost CO_2 reflector shown in Figure 14b. Black arrows indicate prominent examples of tuning: Reflection at the crest of the structure (430 m) tunes at ~50Hz, on mid flank (200m) at ~60 hz and on the far flanks (50m and 760m) at 70-75Hz.

Figure 16 Part of 2D line STO698-06006. a) Seismic section showing picks on the top and base of the top CO_2 layer (for location see Figure 11a). b) Plots of temporal thickness and reflection amplitudes for the seismic section. The blue and red lines show RMS amplitudes extracted from a 4 ms window about the top and base reflector respectively. The filled black circles show the measured peak-trough time separation, while the solid black line and broken black line show temporal thickness estimates derived from spectral decomposition of the 2D line and a coincident (spectrally balanced) 3D seismic profile respectively. Spectral decomposition employed the SPWVD with a sliding 24 point Hanning window.

Figure 17 Normalized iso-frequency sections extracted from the time-frequency distribution computed in a 24 point Hanning window about the topmost CO_2 reflector shown in Figure 16. As frequency increases, the zone of high spectral amplitude moves from the culmination at ~500 m from the origin out to the margins. Black arrows indicate tuning.

Figure 18 a) Schematic of a CO_2-saturated layer sandwiched between different water-saturated lithologies. b) Histogram of reflectivity ratio (~Rtop / R base) for the topmost layer in the central part of line STO698-07001 where the temporal thickness can be measured directly (Figure 14).

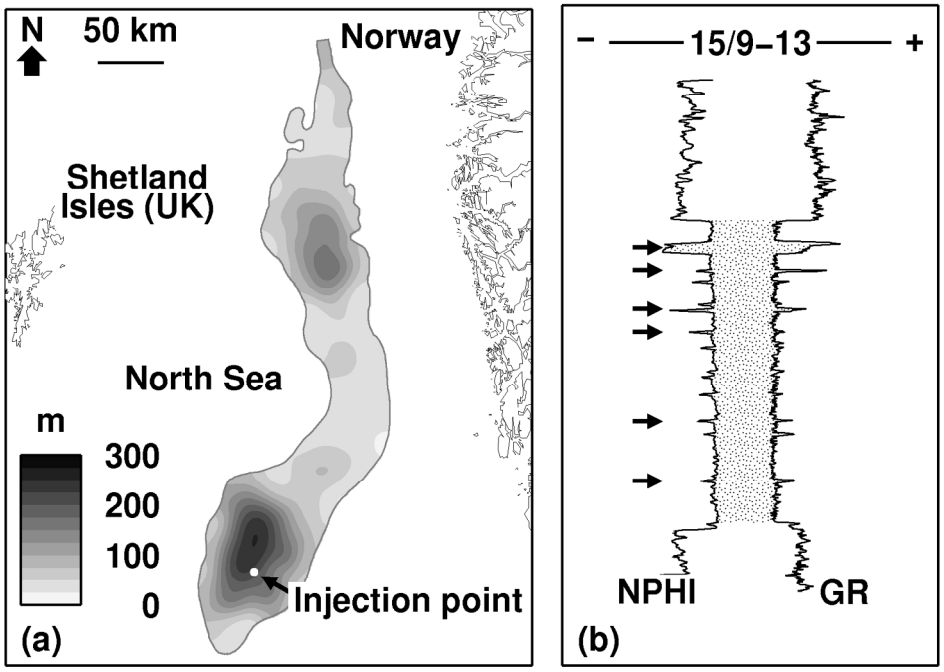
N
50 km
Norway
Shetland
Isles (UK)
North Sea
m
300
200
100
0
Injection point
(a)
–
15/9–13
+
NPHI
GR
(b)

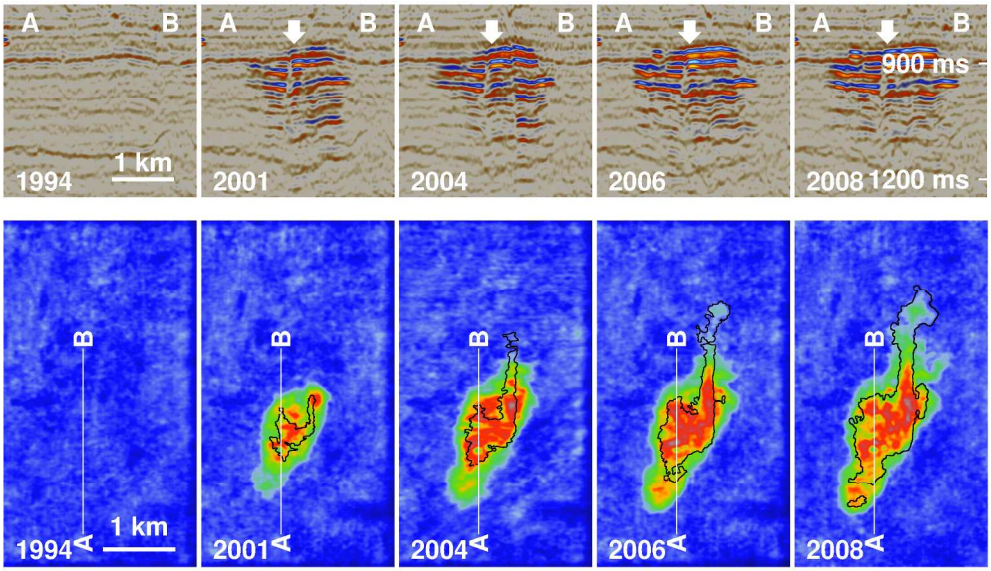

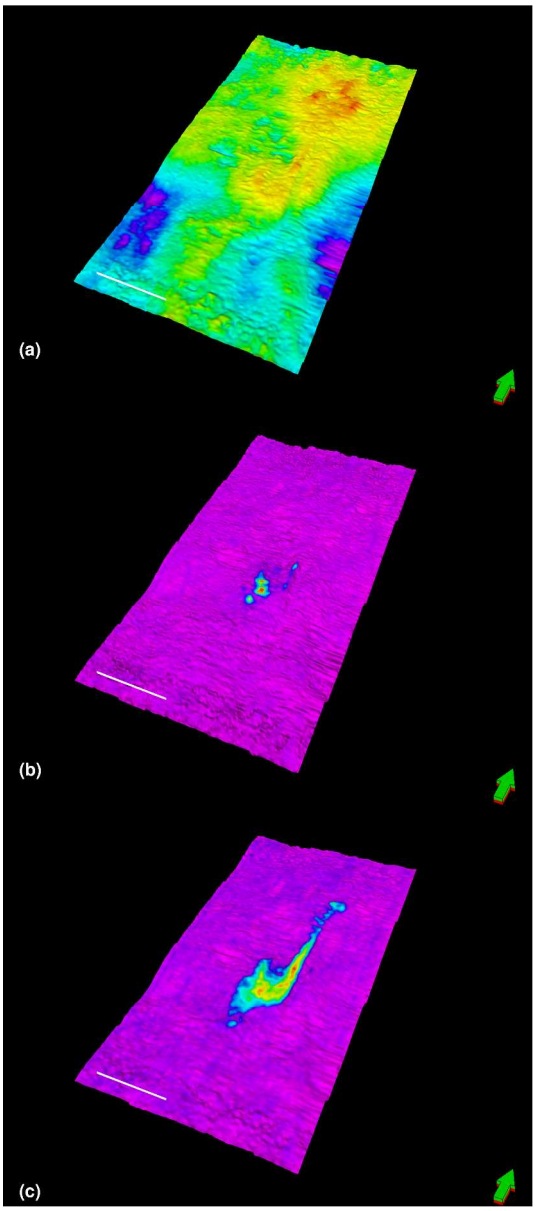
(a)
(b)
(c)

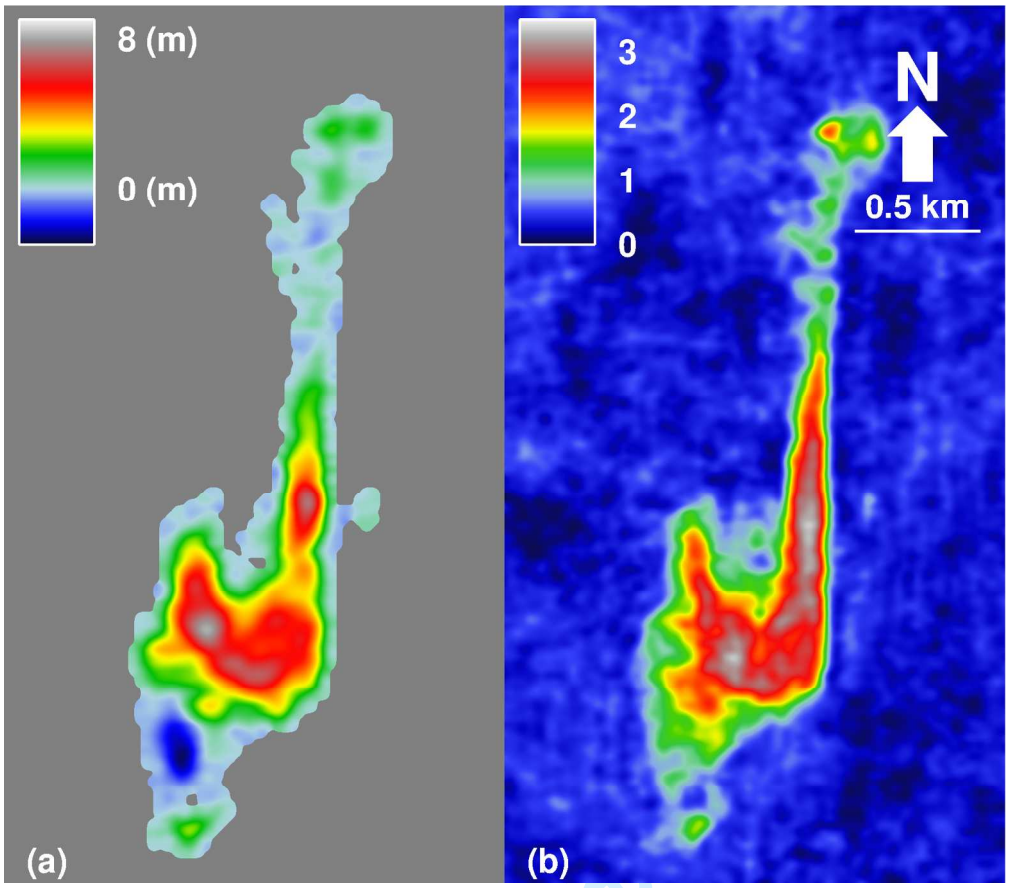

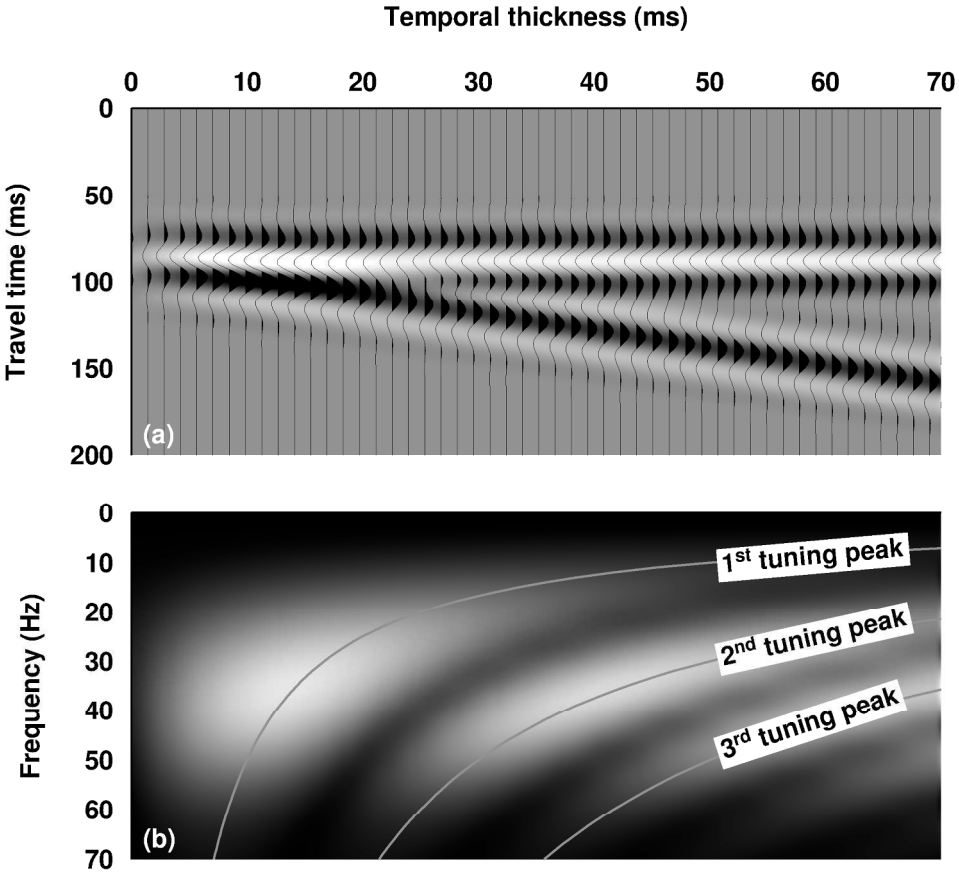
Temporal thickness (ms)
0
10
20
30
40
50
60
70
Travel time (ms)
0
50
100
150
200
(a)
Frequency (Hz)
0
10
20
30
40
50
60
70
1st tuning peak
2nd tuning peak
3rd tuning peak
(b)

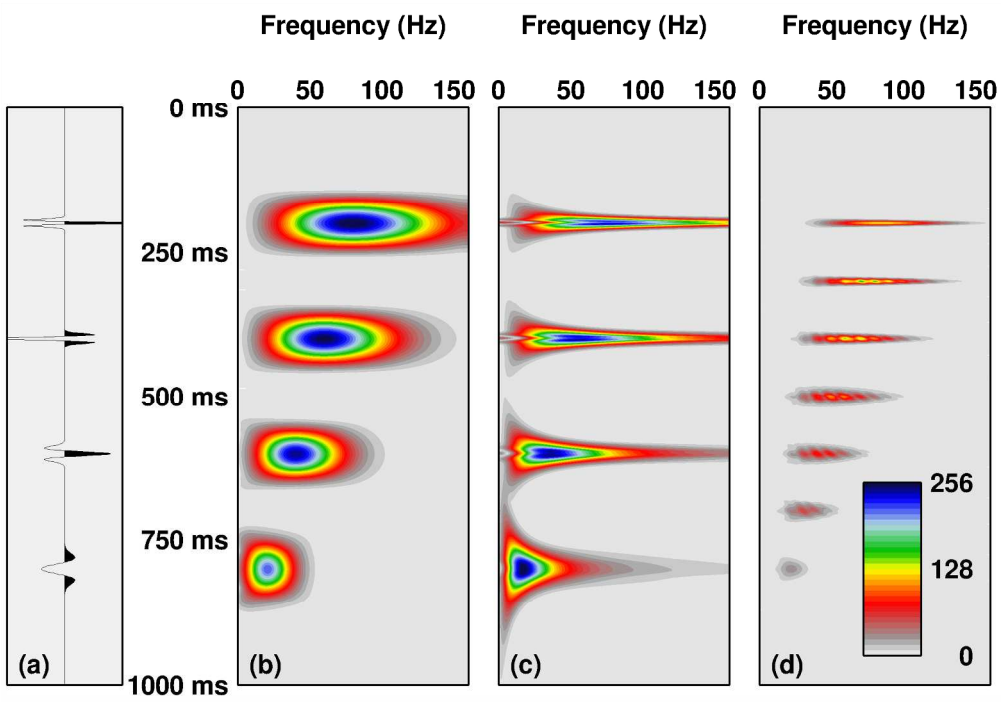

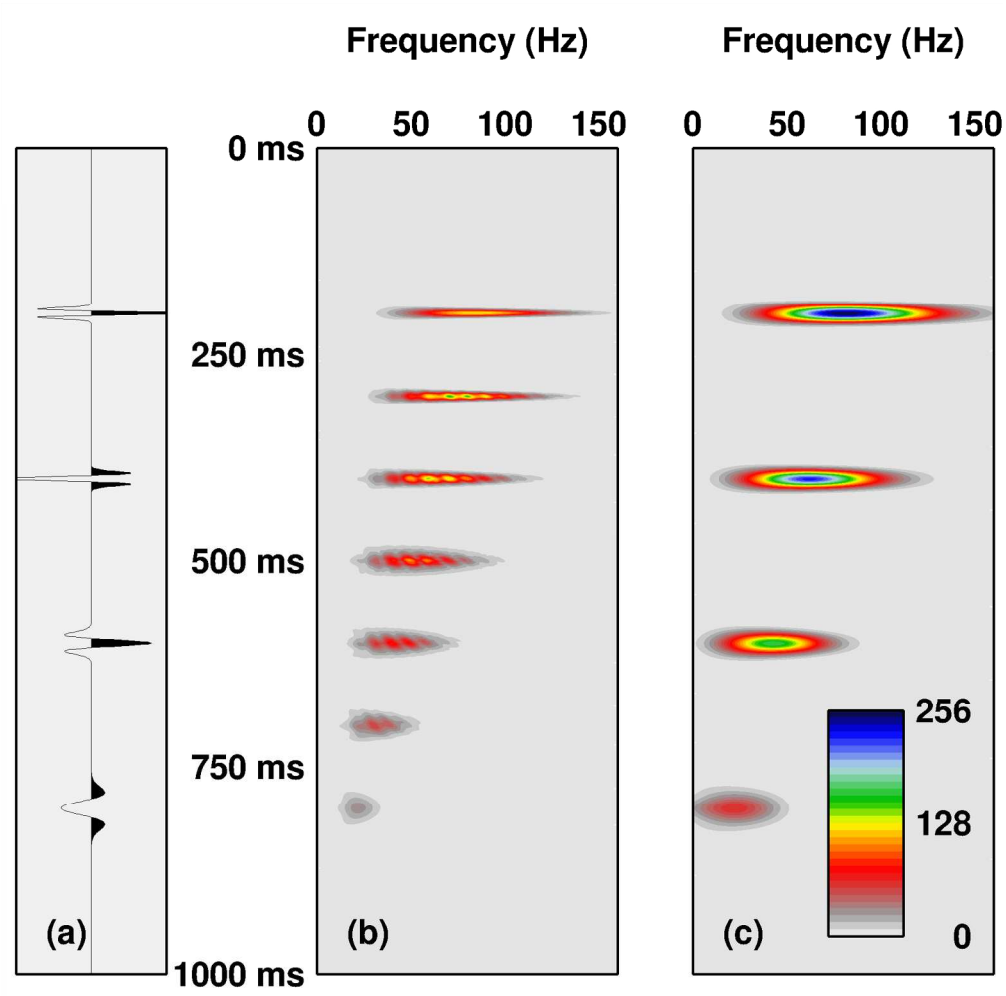
Frequency (Hz)
Frequency (Hz)
0
50
100
150
0
50
100
150
0 ms
250 ms
500 ms
750 ms
1000 ms
(a)
(b)
(c)
256
128
0

Parameter	Value
V_P (mudstone caprock)	2270 ms^{-1}
V_S (mudstone caprock)	850 ms^{-1}
Bulk density (mudstone caprock)	2150 kgm^{-3}
V_P (brine saturated Utsira Sand)	2050 ms^{-1}
V_S (brine saturated Utsira Sand)	620 ms^{-1}
Bulk density (brine saturated Utsira Sand)	2050 kgm^{-3}
Porosity (brine saturated Utsira Sand)	0.37
Brine density	1.040 kgm^{-3}
CO_2 density	690 kgm^{-3}
K_{MATRIX}	36.9 GPa
K_{FLUID}	2.305 GPa
K_{CO2}	0.088 GPa

Table 1 Parameters used to calculate the velocity and density of layers in the synthetic model shown in Figure 9. Initial values (of V_P, V_S and density) for brine-saturated Utsira Sand and the mudstone caprock were averaged from selected well logs close to Sleipner.

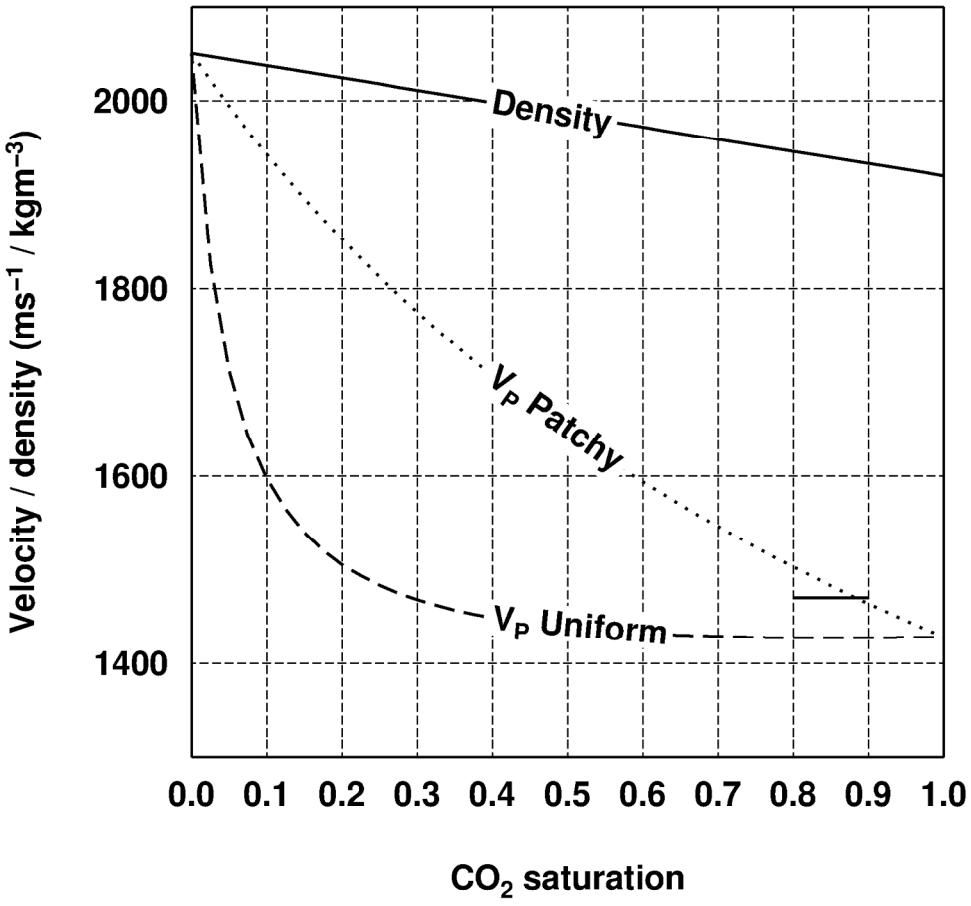
Velocity / density (ms^{-1} / kgm^{-3})
2000
1800
1600
1400
Density
V_P Patchy
V_P Uniform
0.0 0.1 0.2 0.3 0.4 0.5 0.6 0.7 0.8 0.9 1.0
CO_2 saturation

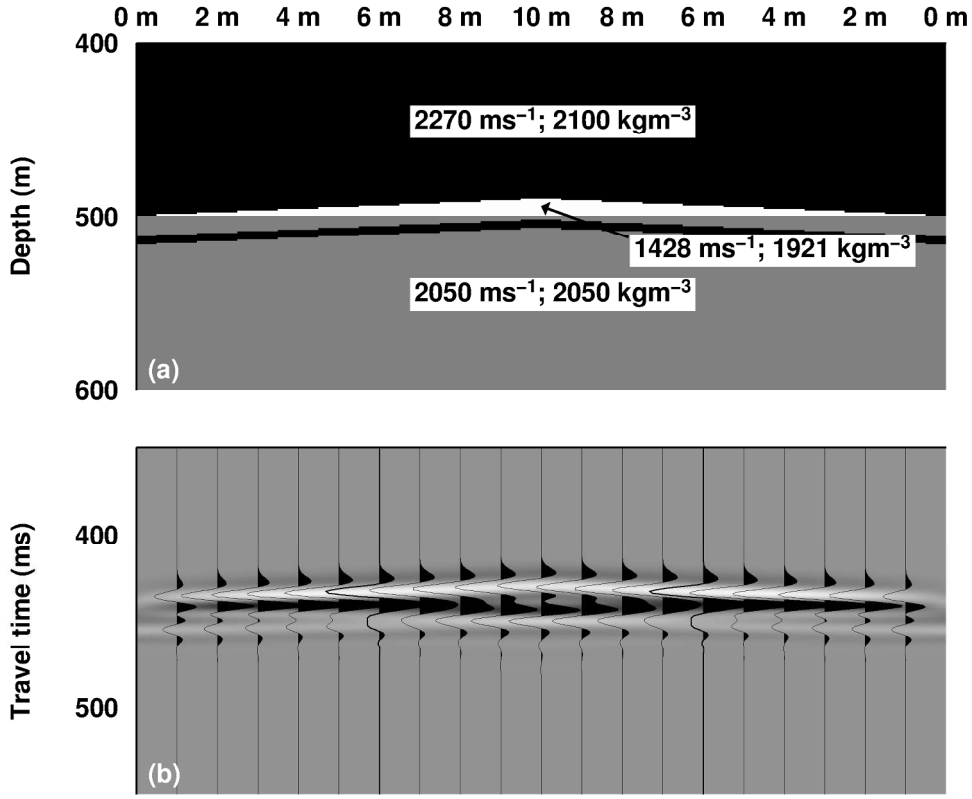
0 m
2 m
4 m
6 m
8 m
10 m
8 m
6 m
4 m
2 m
0 m
400
500
600
Depth (m)
2270 ms−1; 2100 kgm−3
1428 ms−1; 1921 kgm−3
2050 ms−1; 2050 kgm−3
(a)
400
500
Travel time (ms)
(b)

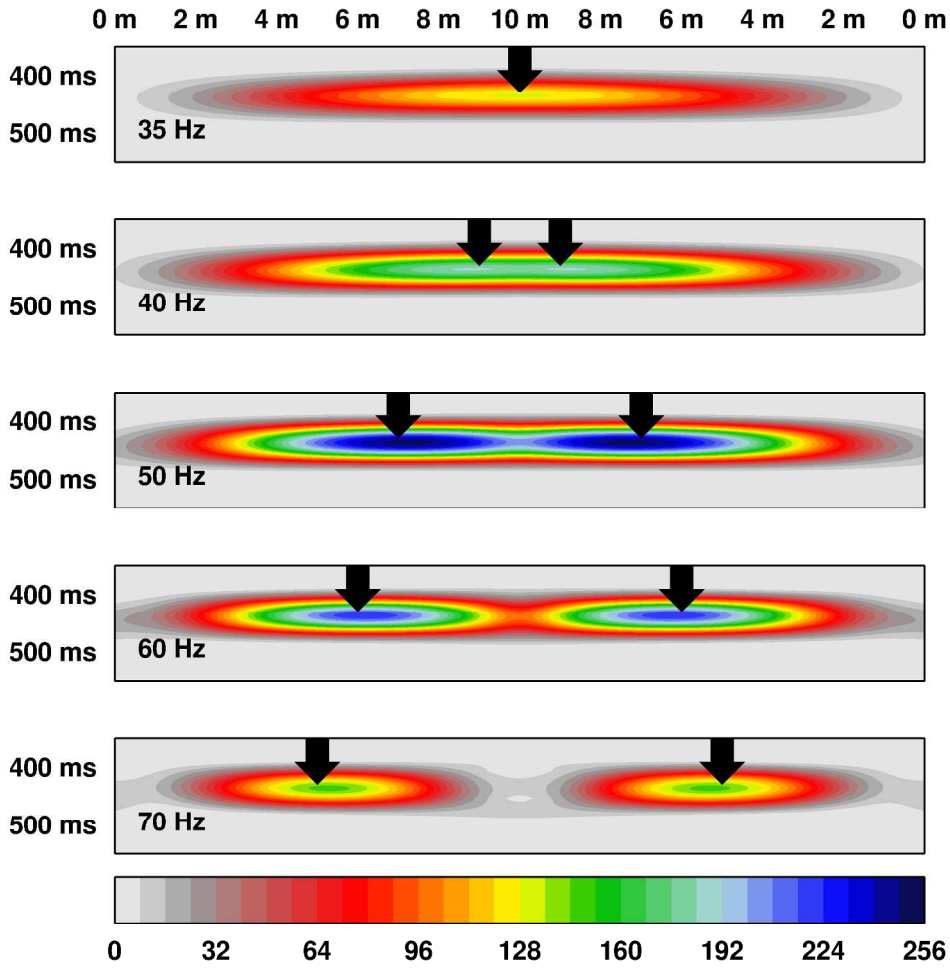
0 m
2 m
4 m
6 m
8 m
10 m
8 m
6 m
4 m
2 m
0 m
400 ms
500 ms
35 Hz
400 ms
500 ms
40 Hz
400 ms
500 ms
50 Hz
400 ms
500 ms
60 Hz
400 ms
500 ms
70 Hz
0
32
64
96
128
160
192
224
256

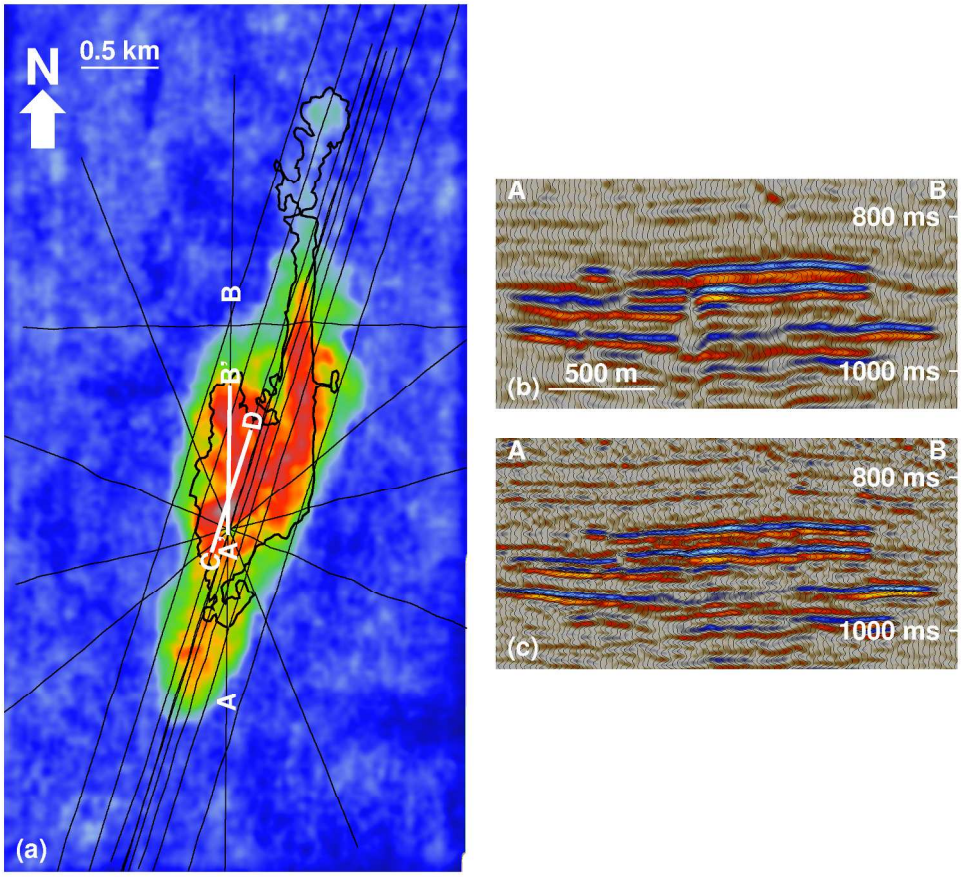

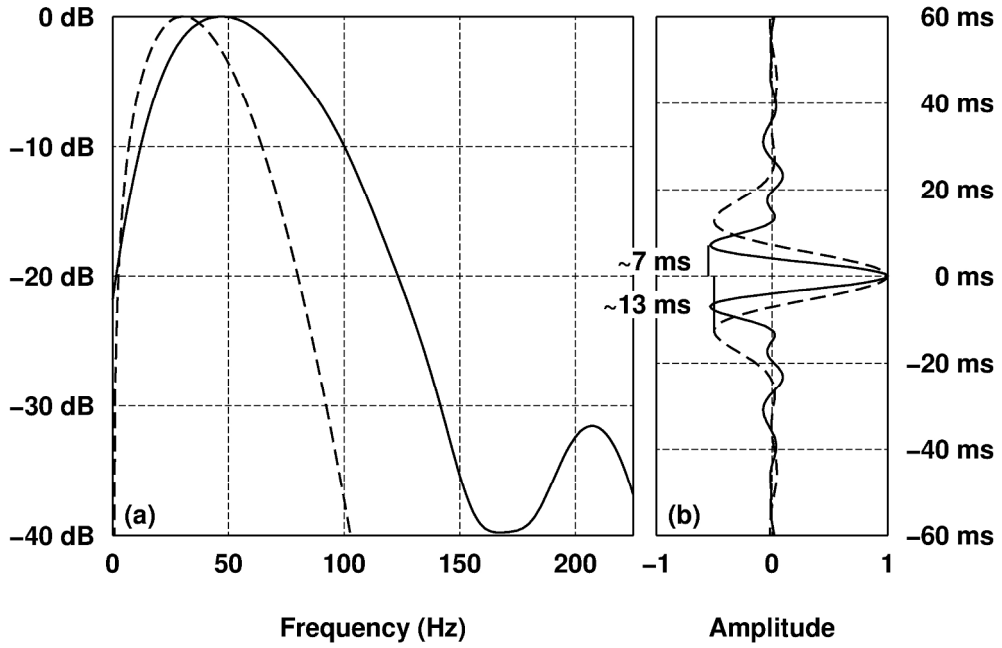
0 dB
–10 dB
–20 dB
–30 dB
–40 dB
(a)
0
50
100
150
200
Frequency (Hz)
~7 ms
~13 ms
(b)
–1
0
1
Amplitude
60 ms
40 ms
20 ms
0 ms
–20 ms
–40 ms
–60 ms

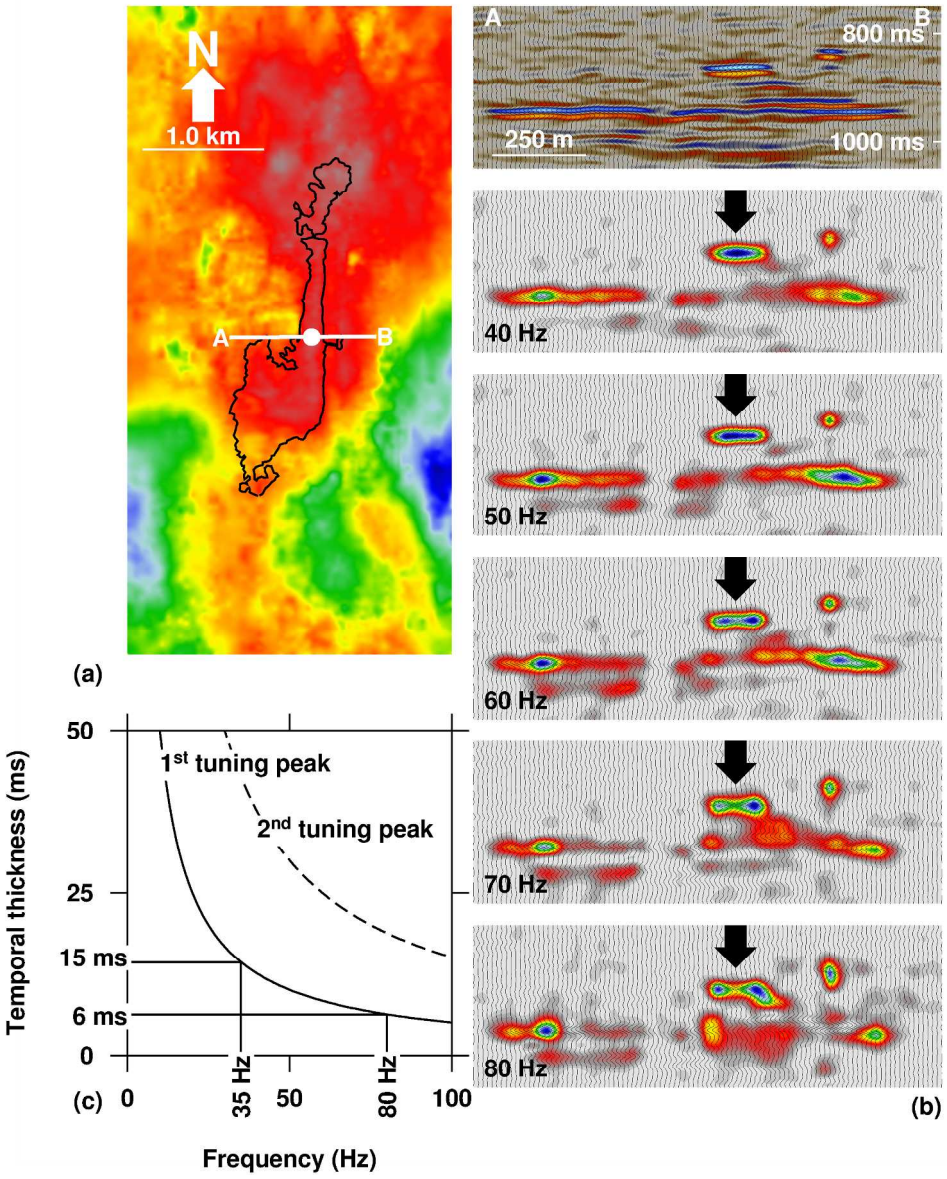
N
1.0 km
A
B
(a)
A
B
800 ms
250 m
1000 ms
40 Hz
50 Hz
60 Hz
70 Hz
80 Hz
(b)
Temporal thickness (ms)
50
25
15 ms
6 ms
0
1st tuning peak
2nd tuning peak
(c) 0
35 Hz
50
80 Hz
100
Frequency (Hz)

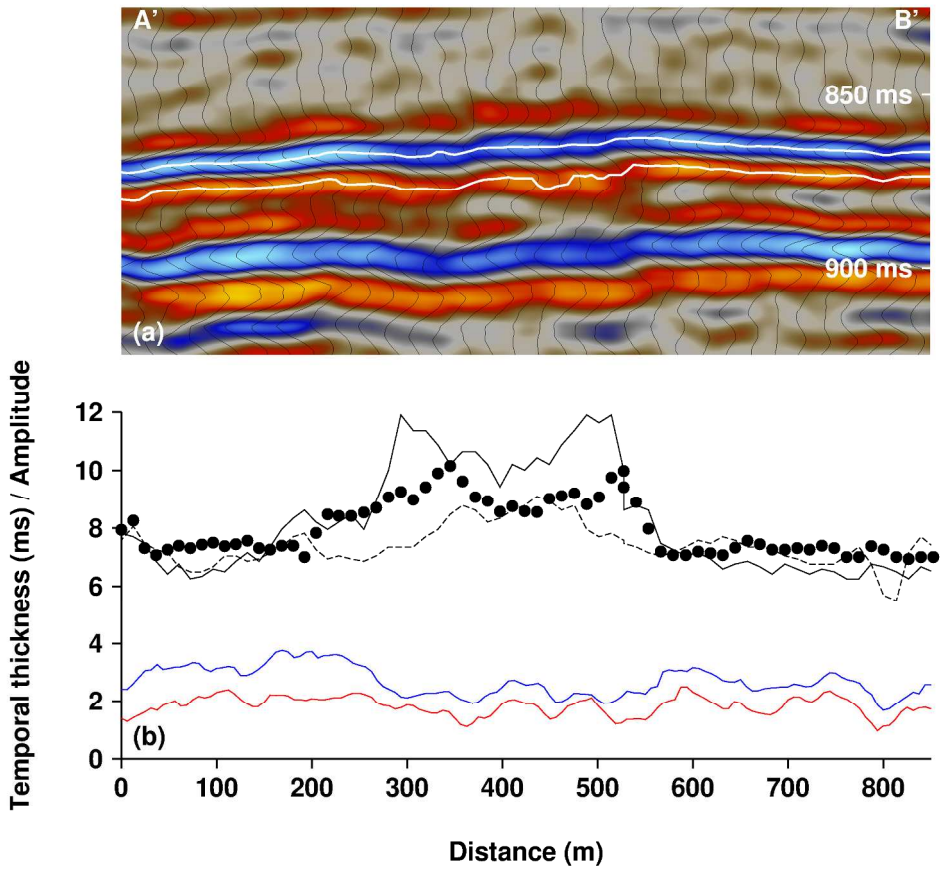
A'
B'
850 ms
900 ms
(a)
Temporal thickness (ms) / Amplitude
12
10
8
6
4
2
0
(b)
0
100
200
300
400
500
600
700
800
Distance (m)

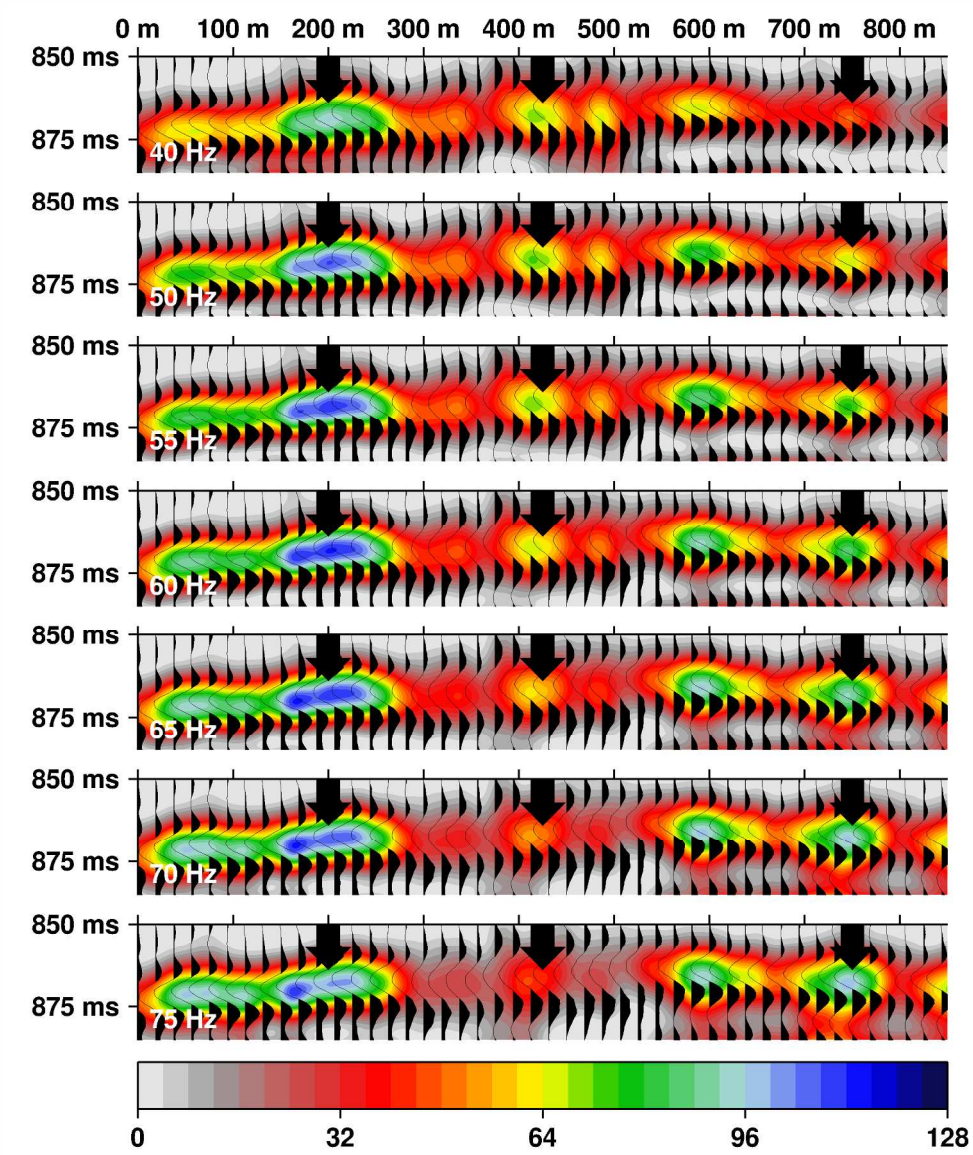
0 m
100 m
200 m
300 m
400 m
500 m
600 m
700 m
800 m
850 ms
875 ms
40 Hz
50 Hz
55 Hz
60 Hz
65 Hz
70 Hz
75 Hz
0
32
64
96
128

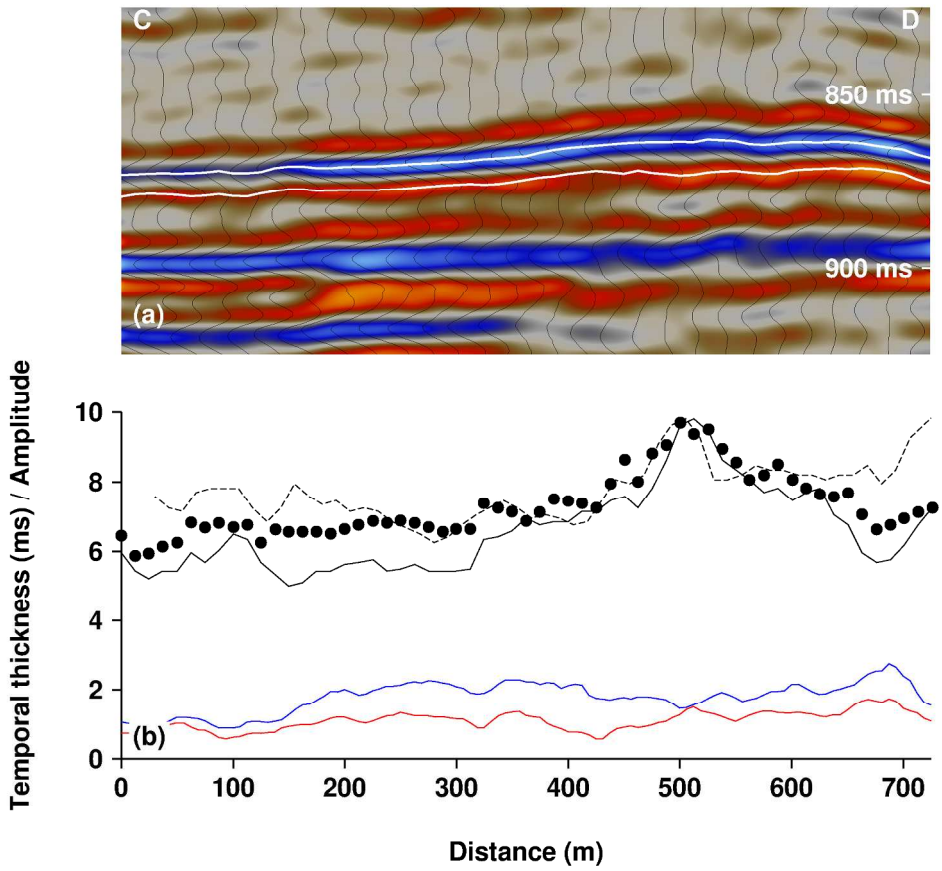
C
D
850 ms
900 ms
(a)
Temporal thickness (ms) / Amplitude
10
8
6
4
2
0
(b)
0
100
200
300
400
500
600
700
Distance (m)

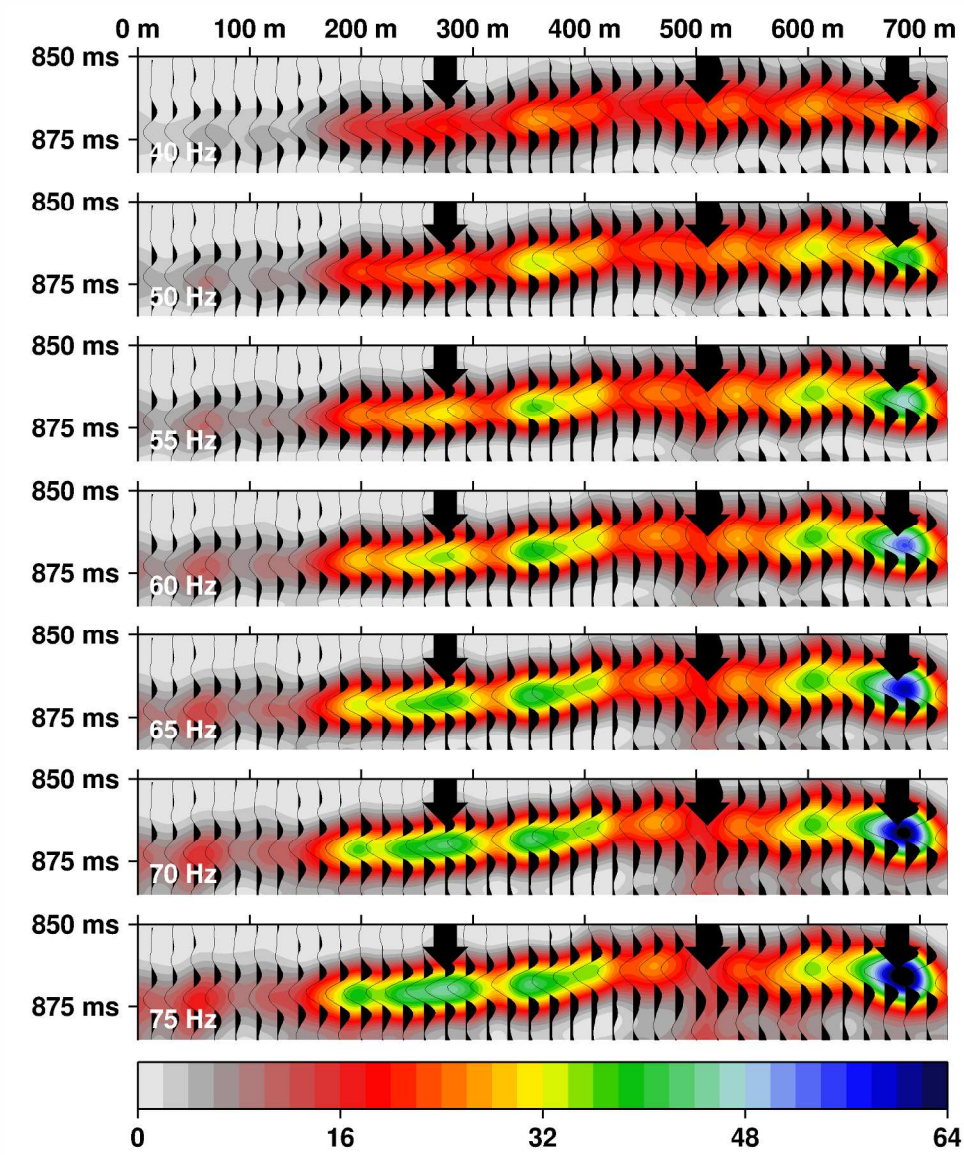
0 m
100 m
200 m
300 m
400 m
500 m
600 m
700 m
850 ms
875 ms
40 Hz
850 ms
875 ms
50 Hz
850 ms
875 ms
55 Hz
850 ms
875 ms
60 Hz
850 ms
875 ms
65 Hz
850 ms
875 ms
70 Hz
850 ms
875 ms
75 Hz
0
16
32
48
64